Journal of Nuclear Materials 493 (2017) 404–411

Contents lists available at ScienceDirect

Journal of Nuclear Materials

journal homepage: www.elsevier.com/locate/jnucmat

Structural investigations of (La,Pu)PO_4 monazite solid solutions: XRD and XAFS study

Yulia Arinicheva [a], Karin Popa [b, *], Andreas C. Scheinost [c], André Rossberg [c], Oliver Dieste-Blanco [b], Philippe Raison [b], Andrea Cambriani [b], Joseph Somers [b], Dirk Bosbach [a], Stefan Neumeier [a, **]

[a] Forschungszentrum Jülich GmbH, Institute of Energy and Climate Research – Nuclear Waste Management and Reactor Safety (IEK-6), D-52425 Jülich, Germany
[b] European Commission, Joint Research Centre, D-76125 Karlsruhe, Germany
[c] Helmholtz-Zentrum Dresden-Rossendorf, Institute of Resource Ecology, D-01314 Dresden, Germany

HIGHLIGHTS

- Single-phase $La_{1-x}Pu_xPO_4$-monazite solid solutions with molar fraction of Pu up to x = 0.15 were synthesized at 1300 °C.
- At a higher Pu content (x = 0.50) residues of unreacted PuO_2 were detected.
- X-ray absorption spectroscopy (XAS) analysis confirms the incorporation of Pu^{III} in the single phase (La,Pu)PO_4 solid solutions.
- $LaPO_4$ local environment is adjusting by the incorporation of Pu, whereas local environment of Pu remains $PuPO_4$-like.

GRAPHICAL ABSTRACT

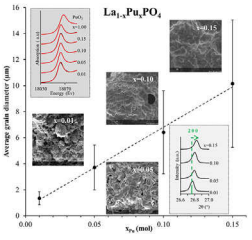

ARTICLE INFO

Article history:
Received 10 February 2017
Received in revised form
21 June 2017
Accepted 28 June 2017
Available online 29 June 2017

Keywords:
Plutonium
Monazite
Waste form
Solid state synthesis
Solid solutions
XRD
EXAFS

ABSTRACT

A solid state method was used to synthesize $La_{1-x}Pu_xPO_4$ (x = 0.01, 0.05, 0.10, 0.15, (0.5)) solid solutions with monazite structure. XRD measurements of the compounds with x = 0.50 revealed the formation of two phases: (La,Pu)PO_4-monazite and a cubic phase (PuO_2). Pure-phase $La_{1-x}Pu_xPO_4$-monazite solid solutions were obtained for materials with x = 0.00–0.15 and confirmed by a linear dependence of the lattice parameters on composition according to Vegard's law. X-ray absorption spectroscopy (XAS) analysis at the Pu-L_{III} and La-L_{III} edges confirmed the +III valence state of plutonium in the monazite solid solutions. The local environment of Pu is $PuPO_4$-like along the solid solution series, except for the longest fitted cation-cation distance, which may be an indication of cluster formation consisting of a few Pu-atoms in the La-Pu-monazite lattice.

* Corresponding author.
** Corresponding author.
E-mail addresses: karin.popa@ec.europa.eu (K. Popa), s.neumeier@fz-juelich.de (S. Neumeier).

http://dx.doi.org/10.1016/j.jnucmat.2017.06.034
0022-3115/

1. Introduction

The strategies for the safe management and disposal of radioactive waste in deep geologic formations include immobilization of radionuclides in a durable waste form as one of the engineered barriers. Various ceramic materials have been proposed as potential waste forms for the immobilization of specific nuclear waste streams, such as separated plutonium from civilian or military sources unsuitable for further use. Among the envisioned immobilization matrices, monazite (monoclinic $LnPO_4$, Ln = La – Gd) appears as a promising candidate [1–4] due to its high structural flexibility [5–8] and specific physico-chemical properties including high chemical durability [5,9–12] as well as high radiation resistance [13–15]. Monazites are also attractive in terms of criticality issues [16]. For the immobilization of fissile ^{239}Pu, stable isotopes of Gd, possessing extremely large neutron-cross-sections ($\sigma(^{157}Gd)$ = 254,000 b), can be incorporated in a tailored $LnPO_4$ host-crystal system.

Phosphate ceramics with monazite structure have been the object of extensive research activities. These studies comprise investigations of the structure and properties and have been performed on the pure $LnPO_4$ endmembers [17–22] and on solid solutions containing mainly surrogates for tri- [11,16,23–26] and tetravalent [27–31] actinides (An).

In contrast only a few studies on transuranium elements-bearing monazite materials are available in the literature. Am- [32,33], Cm- [34–37] as well as Cf-, Bk-, and Es-phosphates [38] have been synthesized and characterized. Monoclinic $PuPO_4$ was obtained originally by Bjorklund [39] by precipitation of Pu^{IV}-oxalatophosphate followed by its thermal decomposition, as well as by dehydration of rhabdophane-like $PuPO_4 \cdot nH_2O$. However a refined crystal structure of the hydrated Pu-phosphate compound as well its XRD pattern have not been reported so far. Therefore it can be assumed, that the "rhabdophane" phase for the precipitation product was suggested in the literature solely analogously to the Ln-rhabdophane [40]. Taking into account the recently reported monoclinic hydrated and two distinct anhydrous (monoclinic and hexagonal) Ln-rhabdophane structures [41,42] further investigations of wet chemical routes for synthesis of actinide-bearing monazite compounds would potentially lead to discovery of new structures of actinide phosphates. The preparation of $Pu^{III}PO_4$-monazite via solid state synthesis from $Pu^{IV}O_2$ and $NH_4H_2PO_4$ in inert atmosphere was reported by Bamberger [43], Glorieux [44] and Bregiroux [37]. Recently the refined crystal structure and oxidation state + III of $PuPO_4$ samples derived by solid state reaction have been solved by Rietveld analysis of XRD data and high resolution X-ray Absorption Near Edge Structure (XANES) spectroscopy, respectively [45]. The thermal behavior of $Pu^{III}PO_4$, such as lattice parameter evolution and decomposition was studied by Jardin et al. [46].

The solid state synthesis route has already been adopted successfully to synthesize $La_{1-x}Pu_xPO_4$ (x = 0.01–0.1) solid solutions by Popa et al. [47] and Zhang et al. [48]. XRD analysis for all compositions revealed single phase materials with monoclinic structure and the oxidation state +III of Pu was confirmed by diffuse reflectance spectroscopy [48]. Finally for self-irradiation studies $PuPO_4$ (7.2 wt% ^{238}Pu) and $(La,Pu)PO_4$ (8.1 wt% ^{238}Pu) were synthesized by wet chemical method based on precipitation from aqueous nitrate solutions by Burakov et al. [49]. However, the incorporation of pure Pu^{IV} by coupled substitution into a monazite-cheralite system $Ln_{1-x}Ca_{0.5x}Th_{0.5x}PO_4$ as well as the synthesis of pure $CaPu^{IV}PO_4$ failed so far. Instead Bregiroux et al. [50] and Deschanels et al. [51] prepared mixed-valence compounds such as $Pu^{III}_{0.4}Pu^{IV}_{0.3}Ca^{II}_{0.3}PO_4$ and $Ca_{0.09}Pu_{0.09}La_{0.73}Th_{0.09}PO_4$, respectively.

Wet chemistry methods, such as precipitation from acidic plutonium solutions after the reprocessing, may offer some advantages over the solid state route by the immobilization of Pu with respect to the safe handling of radionuclides. The drawback of the solid state synthesis methods is an increased contamination risk due to the dust formation, as repeated milling of PuO_2 powder is often necessary to facilitate the plutonium diffusion and thus to obtain homogenous final material. Nevertheless solid state chemistry methods play an important role regarding the immobilization of existing separated inventories of Pu as it is currently stored intermediately as PuO_2. In this case the merits of using the wet chemistry methods vanish taking into account the criticality risks, and thus much smaller industrial batches, as well as the efforts needed to dissolve the hardly soluble PuO_2 in glove boxes. Despite the fact, that PuO_2 is low soluble in aqueous media [52,53] and relatively highly radiation damage resistant [54,55], it should be considered for long term storage as a Pu-bearing solid solution immobilized in an inert matrix rather than in its pure form or as PuO_2-particles dispersed in an inert matrix. The reasons for it are criticality issues, heat emission, He-formation and swelling, leading to the deformation and failure of the waste matrix or/and storage container [55]. Hence, within this work the structural incorporation and loading limitations of Pu^{III} in monazite-type phosphate ceramics by solid state synthesis using PuO_2 as starting material has been investigated systematically for the first time. The refined crystal structure of the $(La,Pu)PO_4$-monazite solid solutions has been studied by a combination of XRD and EXAFS. Particular attention has been paid to the determination of the valence state of plutonium in the solid solution using XANES since $Pu^{IV}O_2$ has been used as precursor material for the solid solution preparation under inert atmosphere.

2. Experimental details

2.1. Synthesis

$La_{1-x}Pu_xPO_4$ solid solutions were synthesized by conventional solid state method under inert atmosphere in order to avoid possible formation of traces of tetravalent plutonium phosphate [31,45]. The synthesis was carried out in alpha-tight glove box designed to handle radioactive materials. Lanthanum oxide (Aldrich. 99.9%), plutonium(IV) oxide (>98% Pu, metal basis), diammonium hydrogen phosphate (Aldrich, 99%) were used as starting reagents without further purification. La_2O_3, PuO_2 in corresponding stoichiometric ratios and $(NH_4)_2HPO_4$ (10% molar excess) were mixed and grinded in an agate mortar. Subsequently the synthesis of the $La_{1-x}Pu_xPO_4$ compounds was performed in inert atmosphere (Ar or N_2) for reduction of Pu^{IV} using the following conditions:

- for the desired molar fraction of Pu x = 0.50: 1000 °C, 1100 °C and 1200 °C, 12 h, Ar-atmosphere with subsequent grinding after each sintering step.
- for the desired molar fraction of Pu x = 0.01, 0.05, 0.10, 0.15: 1300 °C, 5 h, N_2-atmosphere.

By increasing the temperature of the synthesis up to 1300 °C the reaction time was reduced to avoid phosphate decomposition leading to volatile P_4O_{10}. The choice of the synthesis parameters is discussed in detail in the section "Results and discussions".

2.2. X-ray diffraction

The synthesized compounds were characterized by powder X-ray diffraction (PXRD) at room temperature using a Bruker D8

diffractometer mounted in a Bragg-Brentano configuration with a curved Ge (1, 1, 1) monochromator, a ceramic copper tube (40 kV, 40 mA) equipped with a LynxEye position sensitive detector. The data were collected by step scanning in the angle range $10° \leq 2\theta \leq 120°$ with a 2θ step size of 0.0092°. For the measurement, the powder was deposited on a silicon wafer to minimize the background and dispersed on the surface with several drops of isopropanol. The radioactive sample holders were covered by Mylar film to prevent any material dispersal. The phase composition and crystal lattice constants were refined with the Topas software (Bruker AXS GmbH) using the Rietveld technique.

2.3. X-ray absorption fine structure spectroscopy

Powdered samples were diluted with boron nitride powder, pressed into pellets and encapsulated in a double sealed confinement prior the experiment. Pu-L_{III} edge (18057 eV) or La-L_{III} edge (5483 eV) XAFS spectra were collected at ambient temperature at the Rossendorf Beamline (ESRF, Grenoble, France). A water-cooled, 1.4-m long, Rh-coated, meridionally-bent silicon mirror was used for beam collimation into a water-cooled Si(111) double crystal monochromator. The monochromatic beam was then focussed onto the sample by a 1.3-m long, Rh-coated, toroidal silicon mirror, achieving a rejection of higher order harmonics by at least four orders of magnitude. Several spectra were collected in transmission (T) or fluorescence (F) mode using gas-filled ionization chambers and a high-purity, 13-element Ge detector (Canberra) with digital spectrometer (XIA XMap), energy-calibrated using the absorption edge of a simultaneously measured Zr foil (17998 eV) for each sample, and averaged to improve the signal-to-noise ratio using Sixpack [56].

Extended X-ray absorption fine-structure (EXAFS) spectra were extracted from the experimental XAFS spectra using WinXAS [57] following routine procedures. Spectra were normalized by fitting first-order polynomials to the pre-edge and second-order polynomials to the post-edge region, and then converted into k-space by arbitrarily assigning the first edge inflexion point to the onset of kinetic energy of the photoelectron. The EXAFS spectra were then extracted by fitting spline functions to the post-edge region using the auto-background module of WinXAS. The k^3-weighted EXAFS spectra were then Fourier-transformed using a Bessel window with the Bessel parameter set to three. The local structure was determined by shell-fitting (WinXAS) using theoretical phase shift and amplitude functions calculated by FEFF8.2 [58] based on the structure of La monazite [6].

2.4. Scanning electron microscopy with energy dispersive spectroscopy

The actual chemical compositions of the synthetic monazites $La_{1-x}Pu_xPO_4$ with $x = 0.01, 0.05, 0.10, 0.15$ were determined using scanning electron microscopy with energy dispersive spectroscopy (SEM-EDS). The SEM observations were performed on a Philips XL40 SEM (Philips, Amsterdam, Netherlands), which has been adapted for the examination of highly active or irradiated nuclear materials [59,60]: the high voltage unit, column, chamber and turbomolecular pump are mounted inside a glove-box in order to keep the contaminated pieces in a confined space. The primary vacuum system, water cooling circuit and acquisition electronic are placed outside, preventing those parts from contamination by the active samples. The microscope is equipped with Secondary electrons detector (SE) which gives a morphology-related signal, Backscattered electrons detector (BSE) which provides images with Z-related contrast, and Energy dispersive X-ray spectroscopy (EDS) used to obtain elemental analysis of the samples; the beam was always operated at 20 kV. As the samples were in the form of powders, the coating of the same to avoid the electronic charging was not necessary. No further preparation was necessary for the samples.

3. Results and discussions

3.1. Powder X-ray diffraction

The conventional solid state method, reported previously for synthesis of $Pu^{III}PO_4$ with monazite structure [37,45], was applied in this work to obtain $La_{1-x}Pu_xPO_4$ monazite solid solutions according to equation (1).

$$(1-x)La_2O_3 + 2xPu^{IV}O_2 + 2(NH_4)_2HPO_4 \rightarrow 2La_{1-x}Pux^{III}PO_4 + 4NH_3\uparrow + 3H_2O + \tfrac{1}{2}xO_2\uparrow \quad (1)$$

PXRD patterns of the resulted compounds with the corresponding references from COD (Crystallography Open Database) are shown in Fig. 1.

According to the XRD data, the first attempt to synthesize $La_{0.50}Pu_{0.50}PO_4$ solid solution by the conventional solid state method at 1000 °C, led to the formation of several phases: (La,Pu)PO_4 monazite solid solutions with varying Pu-loadings and a cubic PuO_2 phase. The corresponding diffraction pattern (1.a) is shown in Fig. 1, red stars highlight the characteristic Bragg reflections of the PuO_2 phase. The splitting of the (200) Bragg reflections of the monazite phase (insert of Fig. 1) indicates the formation of at least two monazite phases with different molar fractions of Pu. A similar effect was already observed by Bregiroux et al. [19] for mixed lanthanide orthophosphates. It seems to be challenging to obtain a pure and homogeneous monazite phase of mixed orthophosphates by a solid state method due to the differences in reaction kinetics for different cations. In the case of lanthanum and plutonium oxides the differences in reaction kinetics are apparently caused by the reduction of Pu^{IV} during the solid state synthesis. By increasing the synthesis temperature up to 1100 and 1200 °C a single solid solution with monazite structure was obtained, but the PuO_2 Bragg reflections remained evident, too (Fig. 1, diffraction patterns 1.b and 1.c). The phase ratio and lattice parameters of the monazite phase were determined using Rietveld refinement of the XRD data. The increase of temperature from 1100 to 1200 °C led to increase of the monazite phase fraction by 5% reaching 86 ± 1%. However the molar fraction of Pu remained constant within the uncertainties of the refinement (0.15 ± 0.03 and 0.22 ± 0.05, respectively). No further heating has been applied, bearing in mind the thermal behavior of $PuPO_4$ endmember.

The Pu^{IV} to Pu^{III} redox-reaction may inhibit the formation of a pure single phase monazite-type $La_{1-x}Pu_xPO_4$ solid solution by the solid state reaction, especially at higher Pu-content. Moreover it explains the presence of residual PuO_2 after solid state reaction. A

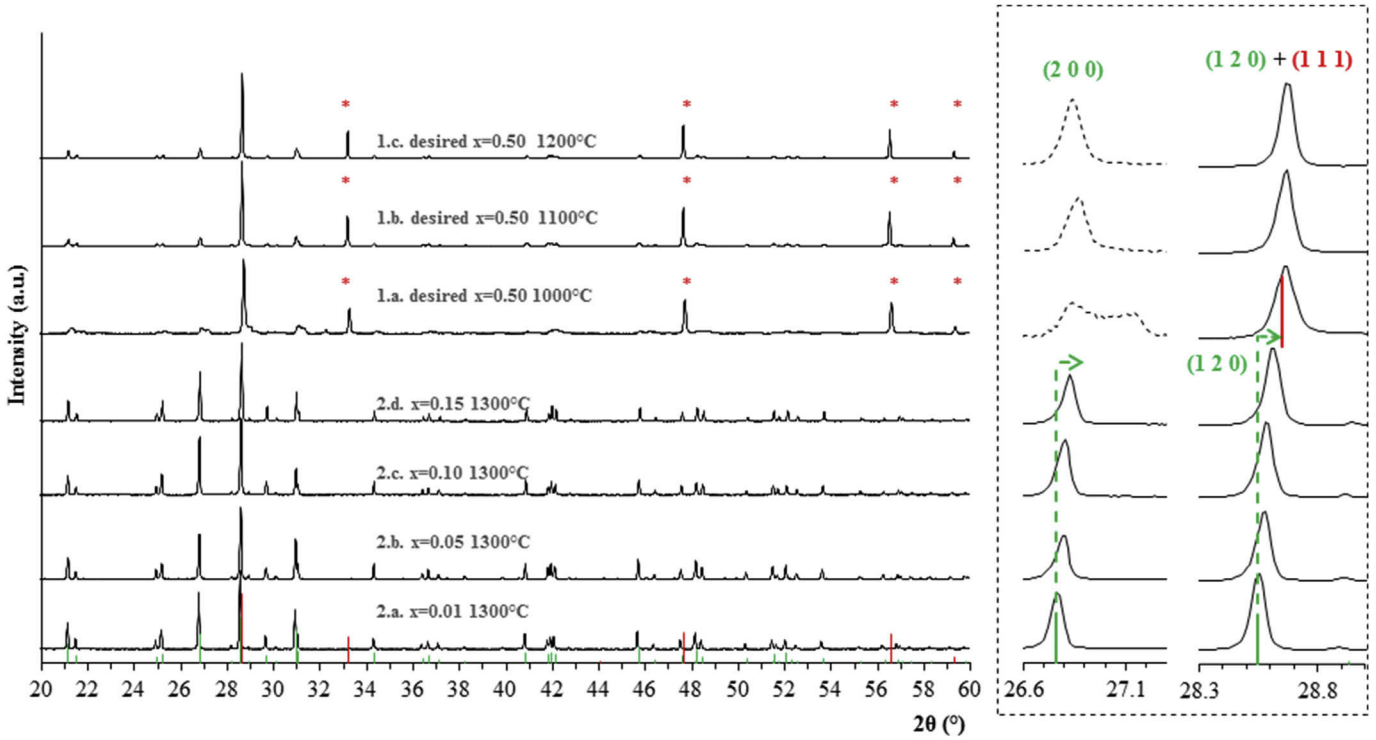

Fig. 1. Diffraction patterns of the synthesized $La_{1-x}Pu_xPO_4$ compounds with x = 0.01, 0.05, 0.1, 0.15, (0.50) with the corresponding references from COD (Crystallography Open Database) for the $LaPO_4$-monazite (green) and PuO_2 (red). Red stars highlight the characteristic Bragg reflections of the PuO_2 phase. The (200) and (120) reflections of the monazite phase are shown in the insert. The (200) Bragg reflections marked with the dashed line are magnified by factor 7 relatively to the corresponding diffraction patterns. (For interpretation of the references to colour in this figure legend, the reader is referred to the web version of this article.)

thermal decomposition of $PuPO_4$ at 1200 °C in inert atmosphere according to Jardin et al. [46] (s. equation (2))

$$4\,PuPO_4 \rightarrow 2\,Pu_2O_3 + P_4O_{10}\uparrow \qquad (2)$$

can definitely be excluded because in detailed evaluation of the XRD patterns no Pu_2O_3 was found. Therefore the residual PuO_2 appears to be unreacted and not reduced precursor material of the synthesis. The formation of a single phase solid solution bearing a higher Pu content can be expected by optimizing the synthesis parameters in terms of the excess of $(NH_4)_2HPO_4$. Additionally, $La_{1-x}Pu_xPO_4$ solid solutions with relatively low molar fraction of Pu might be stabilized by the high thermal stability of the $LaPO_4$ matrix (melting temperature 2072 °C) [61] that would allow for solid state reactions at a temperature above the decomposition temperature of pure $PuPO_4$.

Based on these considerations the target molar fraction of Pu was reduced and pure-phase $La_{1-x}Pu_xPO_4$ solid solutions with monazite structure were successfully obtained at 1300 °C for the compositions with x = 0.01, 0.05, 0.10, 0.15 according to the PXRD data (Fig. 1, diffraction patterns 3.a – d). No characteristic Bragg reflections for PuO_2 are evident in the PXRD patterns. The insert of Fig. 1 demonstrates exemplarily the linear shift of the (200) and (120) Bragg reflections towards higher 2θ values on increasing the Pu-loading. This effect is caused by the lattice contraction due to the incorporation of the slightly smaller Pu^{3+} ions compared to La^{3+} (1.187 Å [45], estimated from David [62], and 1.215 Å [63], respectively (radii are given for a nine-fold coordinated environment)). As a consequence the lattice parameters decrease linearly as a function of Pu-content confirming solid solution formation according to the Vegard's law (Fig. 2). The corresponding refined cell constants are summarized in Table 1.

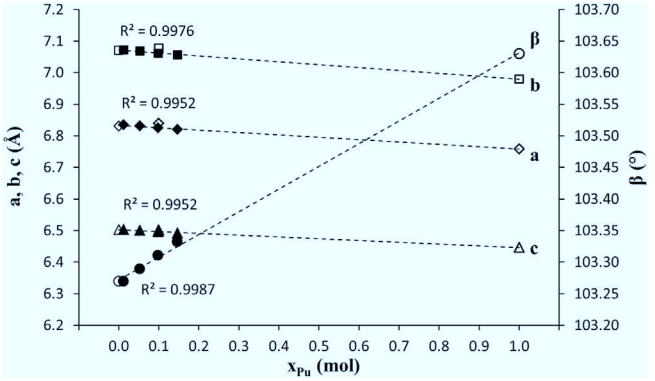

Fig. 2. Evolution of the lattice parameters of the $La_{1-x}Pu_xPO_4$ solid solutions with monazite structure (x = 0–1). Lattice parameters for $LaPO_4$ [6], $PuPO_4$ [3] as well as for $La_{0.9}Pu_{0.1}PO_4$ [47] are marked with open symbols.

The reaction to form a solid solution appears to be more favorable from a kinetic point of view compared to the plutonium phosphate decomposition which possibly starts from 1200 °C. $PuPO_4$ seems to be stabilized at this temperature due to the incorporation into the lattice of the $LaPO_4$ host matrix forming a solid solution.

3.2. Scanning electron microscopy with energy dispersive spectroscopy

The chemical composition and the microstructure of the single phase solid solutions have been investigated using SEM-EDS. The EDS analysis confirmed the homogeneity of the samples as well as the actual compositions of the synthesized solid solutions. The

Table 1
Refined unit cell parameters of the synthesized $La_{1-x}Pu_xPO_4$ solid solutions.

x_{Pu}	a (Å)	b (Å)	c (Å)	β (°)	V (Å^3)
0.01(1)[a]	6.83530(20)	7.07295(20)	6.50377(17)	103.2694(19)	306.035(15)
0.05(0)[b]	6.83161(16)	7.06925(17)	6.50172(16)	103.2890(17)	305.588(13)
0.10(0)[a]	6.82551(20)	7.06221(21)	6.49611(17)	103.3110(20)	304.722(15)
0.15(0)[b]	6.82067(15)	7.05651(16)	6.49266(17)	103.3322(19)	304.071(15)
1 [45]	6.759(1)	6.980(1)	6.447(1)	103.63(1)	295.59
0.1 [47]	6.8396(8)	7.0777(1)	6.5008(2)	103.2(7)	306.38

Mean value of the molar fraction of Pu derived from [a]3 and [b]2 EDS measurements.

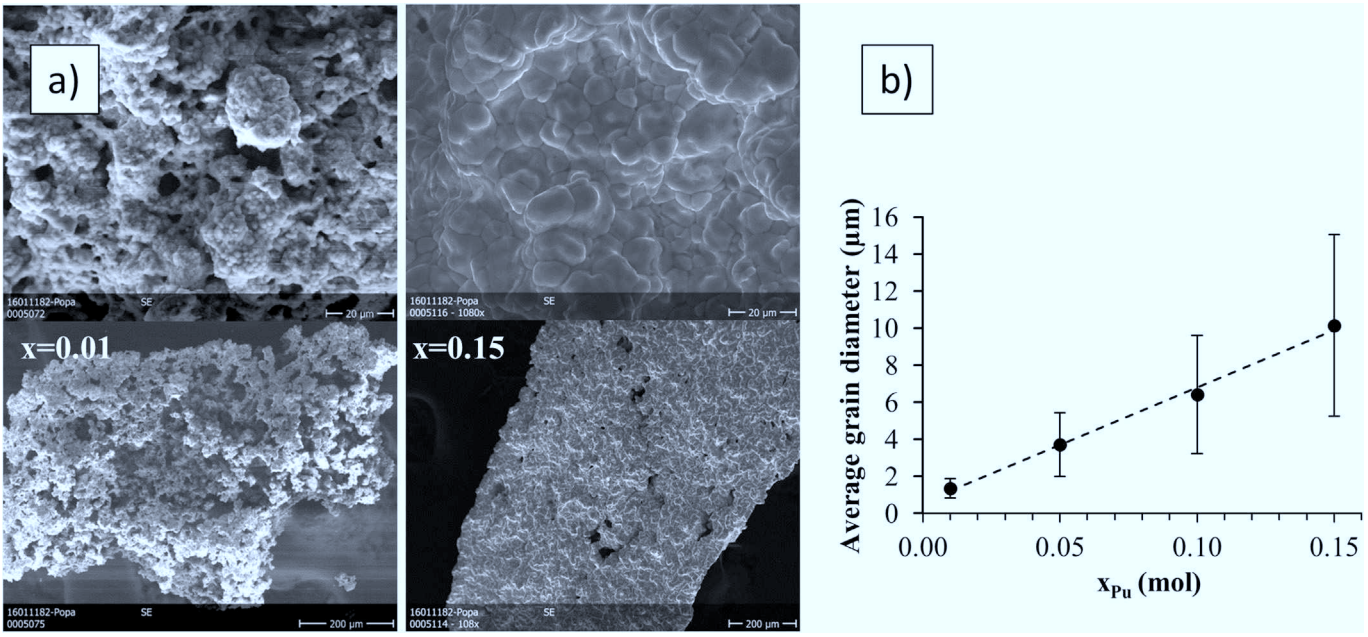

Fig. 3. SEM images of microstructure (a) and average grain diameters (b) of the $La_{1-x}Pu_xPO_4$ solid solutions with monazite structure in dependence on composition. The apparent increasing error bars with increasing Pu content represent the uncertainties of a grain size distribution.

resulting molar fraction of Pu is given in Table 1.

The SEM-micrographs in Fig. 3a) show the microstructures of the selected compounds with x = 0.01 and x = 0.15 at different magnifications. The sponge-like microstructure of the samples indicates a vigorous reaction during the heat treatment accompanied by active gas release. These observations confirmed self-homogenization of the reaction mixture during the heat treatment. The average grain diameter for each composition determined from the corresponding SEM micrographs is presented in Fig. 3b) as a function of composition. It is noticeable, that the grains for the composition with the molar fraction of plutonium x = 0.15 are larger whereas its porosity is smaller in comparison to those for x = 0.01 (Fig. 3a). A linear increase in the average grain diameter with increasing molar fraction of plutonium was observed. It suggests that Pu content increases the grain growth rate of the solid solutions at the given temperature.

3.3. X-ray absorption spectroscopy

The Pu-L_{III} edge X-ray absorption near-edge structure (XANES) spectra of the synthesized solid solutions (x = 0.01, 0.05, 0.10, 0.15) are presented in Fig. 4. The white line position of the solid solutions matches that of the purely trivalent monazite endmember (x = 1.00), and is about 5 eV lower than that of the Pu^{IV} reference PuO_2. A subsequent analysis of the spectral series by iterative transformation factor analysis (ITFA) [64,65] confirmed that all

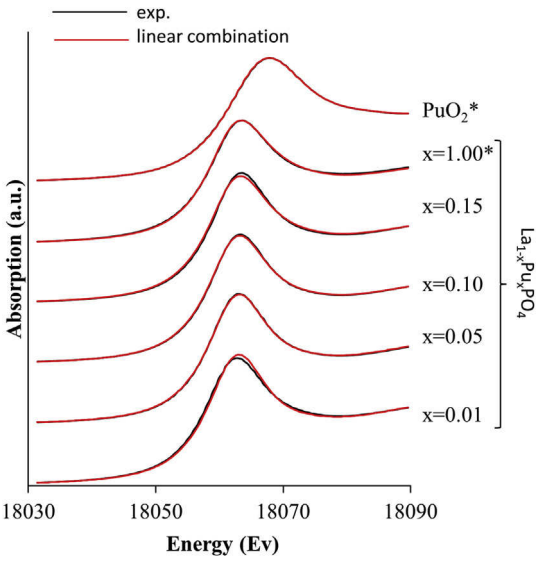

Fig. 4. Experimental Pu-L_{III} XANES spectra (black) and their reproduction (red) by the two reference spectra show on top (Pu^{III} and Pu^{IV}). (For interpretation of the references to colour in this figure legend, the reader is referred to the web version of this article.)

samples contain at least 95% of Pu^{III}, as expected for the synthesis under inert atmosphere [46].

The atomic environment of the incorporated Pu atoms in the crystal structure has been studied as a function of composition of the synthesized solid solutions (x = 0.01, 0.05, 0.10, 0.15) by extended X-ray absorption fine-structure (EXAFS) spectroscopy.

Fig. 5 shows from top to bottom the Pu-L_{III} edge Fourier transform magnitudes (FTM) of the pure Pu-monazite endmember, of the Pu-doped La-monazite samples sorted along decreasing Pu molar fraction, and finally the La-L_{III} spectrum of the pure La-monazite endmember. The FTM of the Pu-La series are almost identical independent of Pu-doping; while the FTM of pure Pu-monazite has distinct features in the regions of the next P neighbors (marked in orange) and of the next Pu/La neighbors (marked in purple). In contrast, the spectrum of $LaPO_4$ shows a longer distance of the oxygen coordination shell (red), in addition to different peak shapes in the P and Pu/La regions.

With space group P 1 21/n 1(14), the monazite structure shows poor radial distribution ordering of the atoms around the cation centers. In $LaPO_4$, for instance, the coordination shell of nine oxygen atoms has La-O distances (R_{La-O}) ranging from 2.45 to 2.78 Å; the seven P atoms from the phosphate units directly linked to this LaO_9 polyhedron have distances ranging from 3.20 to 3.79 Å, followed by 3 La neighbors from 4.08 to 4.15 Å and another three La neighbors from 4.30 to 4.36 Å. Since the distal resolution of EXAFS is limited by $\pi/(2^*\Delta\chi)$, shells have to be separated by at least 0.21 Å, given the limited k-range available (2.0–9.5 Å). Therefore, the different individual interatomic distances had to be grouped into shells for EXAFS fitting. The most stable fits were obtained with the following grouping: a coordination shell of 9 oxygen atoms, 3 shorter and 4 longer cation-P distances, 3 shorter and 3 longer cation-cation distances. The results derived from the corresponding fits are shown in Table 2.

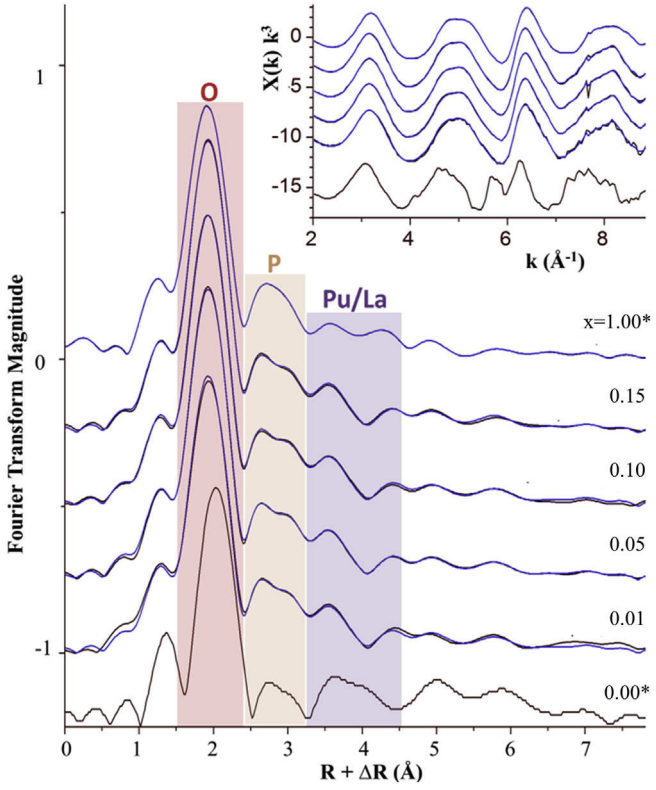

Fig. 5. Pu-L_{III} EXAFS spectra of Pu monazite and Pu-La monazite solid solutions in comparison to the La-L_{III} EXAFS spectrum of La monazite. Experimental data are given as black lines, blue lines are the reconstruction of the Pu-L_{III} spectra by two principal components. The large figure gives the k^3-weighted Fourier transform magnitudes (FTM), the insert the k^3-weighted chi-spectra. Major contributions from the nine coordinating oxygen atoms are within the red area, those of the seven nearest phosphorous atoms are within the orange area, and those of the six nearest Pu/La atoms are within the purple area. (For interpretation of the references to colour in this figure legend, the reader is referred to the web version of this article.)

In all Pu-containing monazites, the coordination shell could be fitted with 9 Pu-O paths, giving average distances of 2.47–2.48 Å and a relatively high local disorder expressed by Debye-Waller factors of ~0.01 $Å^2$ in line with the expected distorted tricapped prism structure (Table 2). For $LaPO_4$, this distance is significantly larger (2.53 Å), owing to the larger ionic radius of La^{3+} versus Pu^{3+}. Furthermore, the two Pu-P paths provided distances at 3.20 and 3.74 Å, with no significant change of distances or disorder from 100% to 1% Pu.

For $PuPO_4$, the following two Pu-Pu shells were fitted with average distances of 4.07 and 4.24 Å, well in line with the monazite structural model. For the Pu-La solid solution series, however, the backscattering elements of the shorter and longer cation-cation interactions may be La or Pu, with a prevalence of Pu-Pu for high Pu content, and a prevalence of Pu-La for lower Pu. We tried to identify the prevalent backscattering element by wavelet analysis [66], but could not distinguish contributions from La and Pu due to the k range (2.0–9.5 Å) limited by the presence of the Am daughter nuclide. We therefore tried different combinations of Pu-Pu and Pu-La paths. For all samples, with the molar fraction of Pu ranging from

Table 2
EXAFS shell fit results of Pu-doped La-monazites in comparison to $PuPO_4$ and $LaPO_4$ (Pu-L_{III} and La-L_{III} spectra, respectively).

Sample	Path	CN	R [Å]	σ^2 [$Å^2$]	ΔE_0 [eV]	S_0^2	χ_{res} [%]
$PuPO_4$	Pu-O	9	2.47	0.0103	9.9	0.70	7.4
(T)	Pu-P	3	3.21	0.0117			
	Pu-P	4	3.74	0.0105			
	Pu-Pu	3	4.07	0.0061			
	Pu-Pu	3	4.24	0.0057			
$La_{0.85}Pu_{0.15}PO_4$	Pu-O	9	2.48	0.0094	9.2	0.77	6.3
(T)	Pu-P	3	3.20	0.0122			
$La_{0.90}Pu_{0.10}PO_4$	Pu-P	4	3.75	0.0083			
(T)	Pu-Pu	3	4.10	0.0014			
	Pu-La	3	4.33	0.0010			
	Pu-O	9	2.48	0.0098	8.9	0.79	6.3
	Pu-P	3	3.20	0.0125			
	Pu-P	4	3.74	0.0085			
	Pu-Pu	3	4.05	0.0016			
	Pu-La	3	4.32	0.0010			
$La_{0.95}Pu_{0.05}PO_4$	Pu-O	9	2.48	0.0094	8.8	0.78	6.6
(T)	Pu-P	3	3.20	0.0130			
	Pu-P	4	3.74	0.0082			
	Pu-Pu	3	4.06	0.0014			
	Pu-La	3	4.33	0.0010			
$La_{0.99}Pu_{0.01}PO_4$	Pu-O	9	2.48	0.0100	9.2	0.74	7.6
(F)	Pu-P	3	3.20	0.0112			
	Pu-P	4	3.74	0.0083			
	Pu-Pu	3	4.06	0.0012			
	Pu-La	3	4.33	0.0010			
$LaPO_4$	La-O	9	2.53	0.0106	10.2	0.63	13.8
(F)	La-P	3	3.31	0.0205[c]			
	La-P	4	3.73	0.0205[c]			
	La-La	3	4.08	0.0082[c]			
	La-La	3	4.38	0.0082[c]			
$LaPO_4$	La-O	9	2.56				
(XRD) [6]	La-P	3	3.32				
	La-P	4	3.76				
	La-La	3	4.11				
	La-La	3	4.32				

CN: coordination number, R: radial distance, σ^2: Debye-Waller term, ΔE_0: phase shift, S_0^2: amplitude reduction factor, χ_{res}: residual error, c: parameters were correlated during the EXAFS fit, T, F: EXAFS data collected in transmission or fluorescence mode, respectively.

1 to 15, the best fit was obtained with Pu-Pu paths for the shorter, and Pu-La paths for the longer distance. This may be an indication for an inhomogeneous distribution of Pu in the La-Pu-monazite lattice, i.e. a certain clustering of Pu cations, which changes little as is revealed by the invariant FTM pattern in the La/Pu region. With R_{Pu-Pu} between 4.05 and 4.10 Å, the solid solution samples do not vary significantly from the distance of 4.07 Å found for the pure $PuPO_4$ endmember, further supporting the clustering of Pu atoms. In contrast, the Pu-La distances at 4.33 Å are significantly longer than the corresponding Pu-Pu distance of 4.24 Å in $PuPO_4$, and similar to the La-La distance in $LaPO_4$.

In conclusion, the local environment of Pu remains $PuPO_4$-like along the solid solution series, except for the longest fitted cation-cation distance, which is always $LaPO_4$-like. Such an effect is most consistently explained by clustering, i.e. a heterogeneous distribution of cations in solid solutions at the molecular scale, which is observable by short-range probes like EXAFS, but not by long-range probes like XRD as was observed for instance for metal oxides, silicates and phosphates [67–74]. Even more relevant, a similar effect was recently observed by EXAFS for (La,Eu)PO_4 and Cm-doped (La,Gd)PO_4 monazite solid solutions, where Eu or Gd served as inactive surrogates for trivalent actinides [75,76]. For both solid solution series bond lengths in the local environment of Eu and Cm, respectively were significantly shorter in comparison to those in the local environment of La. This indicates that the local environment of La with relatively longer and therefore weaker bonds is adjusting by the incorporation of smaller cations in the $LaPO_4$ monazite matrix.

4. Conclusions

Single-phase $La_{1-x}Pu^{III}_xPO_4$-monazite solid solutions with molar fraction of Pu up to $x = 0.15$ were synthesized by a solid state method at 1300 °C. At a higher Pu content ($x = 0.50$) residues of unreacted PuO_2 were detected. Due to the absence of Pu_2O_3, however, decomposition of formed $PuPO_4$ or associate solid solution can be excluded. Moreover the formation of single phase solid solutions with higher Pu content can be expected after optimization of synthesis method. XRD and SEM analysis the solid solutions are found to be single phase and homogeneous. X-ray absorption spectroscopy (XAS) analysis of the single phase (La,Pu)PO_4 solid solutions at the Pu-L_{III} and La-L_{III} edges proves the incorporation of Pu^{III} into defined lattice sites of the monazite structure and indicates clustering of few Pu atoms in the La-Pu-monazite lattice. Comparison of XRD and EXAFS data reveals adjusting of $LaPO_4$ local environment by incorporation of Pu, whereas local environment of Pu remains $PuPO_4$-like for the entire solid solution range. This work demonstrates that monazite-type ceramics with a reasonable amount of Pu (10–15%) for nuclear waste applications can be fabricated by conventional solid state reaction at 1300 °C.

Funding sources

This work has been supported by the European FP7 TALISMAN project (JRP-No.: TALI-C06-11) under contract with the European Commission, the German Federal Ministry of Education and Research (BMBF; grant-no: 02NUK021A and 02NUK021B) and the HITEC – the Graduate School in Energy and Climate Research at the Forschungszentrum Jülich.

Acknowledgment

We are very grateful to Mr Daniel Bouëxière for the performance of the XRD measurements.

References

[1] R.C. Ewing, L.M. Wang, Phosphates as nuclear waste forms, Rev. Min. Geochem 48 (2002) 673–699.
[2] G.R. Lumpkin, Ceramic waste forms for actinides, Elements 2 (2006) 365–372.
[3] E.H. Oelkers, J.-M. Montel, Phosphates and nuclear waste storage, Elements 4 (2008) 113–116.
[4] H. Schlenz, J. Heuser, A. Neumann, S. Schmitz, D. Bosbach, Monazite as a suitable actinide waste form, Z. Krist. 228 (2013) 113–123.
[5] N. Dacheux, N. Clavier, R. Podor, Monazite as a promising long-term radioactive waste matrix: benefits of high-structural flexibility and chemical durability, Am. Mineral. 98 (5–6) (2013) 833–847.
[6] Y.X. Ni, J.M. Hughes, A.N. Mariano, Crystal chemistry of the monazite and xenotime structures, Am. Mineral. 80 (1–2) (1995) 21–26.
[7] L.A. Boatner, Synthesis, structure, and properties of monazite, pretulite, and xenotime, Rev. Mineral. Geochem. 48 (2002) 87–121.
[8] N. Clavier, R. Podor, N. Dacheux, Crystal chemistry of the monazite structure, J. Eur. Ceram. Soc. 31 (2011) 941–976.
[9] E.H. Oelkers, F. Poitrasson, An experimental study of the dissolution stoichiometry and rates of a natural monazite as a function of temperature from 50 to 230 °C and pH from 1.5 to 10, Chem. Geol. 191 (2002) 73–87.
[10] G. Deissmann, S. Neumeier, G. Modolo, D. Bosbach, Durability of potential plutonium wasteforms under repository conditions, Mineral. Mag. 76 (8) (2012) 2911–2918.
[11] F. Brandt, S. Neumeier, T. Schuppik, Y. Arinicheva, A. Bukaemskiy, G. Modolo, D. Bosbach, Conditioning of minor actinides in lanthanum monazite ceramics: a surrogate study with europium, Prog. Nucl. Energy 72 (2014) 140–143.
[12] C. Gausse, S. Szenknect, D.W. Qin, A. Mesbah, N. Clavier, S. Neumeier, D. Bosbach, N. Dacheux, Determination of the solubility of rhabdophanes $LnPO_4 \cdot 0.667H_2O$ (Ln = La to Dy), Eur. J. Inorg. Chem. (2016) 4615–4630.
[13] A. Meldrum, L.A. Boatner, R.C. Ewing, Radiation damage in zircon and monazite, Phys. Rev. B 56 (1997) 13805–13814.
[14] W.J. Weber, A. Navrotsky, S. Stefanovsky, E. Vance, E. Vernaz, Materials science of high-level nuclear waste immobilization, MRS Bull. 34 (2009) 46–53.
[15] R. Ewing, W. Weber, F. Clinard, Radiation effects in nuclear waste forms for high-level radioactive waste, Prog. Nucl. Energ 29 (1995) 63–127.
[16] O. Terra, N. Clavier, N. Dacheux, R. Podor, Preparation and characterization of lanthanum–gadolinium monazites as ceramics for radioactive waste storage, New J. Chem. 27 (2003) 957–967.
[17] D. Bregiroux, S. Lucas, E. Champion, F. Audubert, D. Bernache-Assollant, Sintering and microstructure of rare earth phosphate ceramics $REPO_4$ with RE = La, Ce or Y, J. Eur. Ceram. Soc. 26 (2006) 279–287.
[18] K. Popa, R.J.M. Konings, High-temperature heat capacities of $EuPO_4$ and $SmPO_4$ synthetic monazites, Thermochim. Acta 445 (1) (2006) 49–52.
[19] D. Bregiroux, F. Audubert, T. Charpentier, D. Sakellariou, D. Bernache-Assollant, Solid-state synthesis of monazite-type compounds LnPO4 (Ln = La to Gd), Solid State Sci. 9 (2007) 432–439.
[20] J. Heuser, A.A. Bukaemskiy, S. Neumeier, A. Neumann, D. Bosbach, Raman and infrared spectroscopy of monazite-type ceramics used for nuclear waste conditioning, Prog. Nucl. Energ 72 (2014) 149–155.
[21] S.V. Ushakov, K.B. Helean, A. Navrotsky, L.A. Boatner, Thermochemistry of rare-earth orthophosphates, J. Mater. Res. 16 (9) (2001) 2623–2633.
[22] N. Huittinen, Y. Arinicheva, M. Schmitz, S. Neumeier, T. Stumpf, Using Eu^{3+} as an atomic probe to investigate the local environment in $LaPO_4$–$GdPO_4$ monazite end-members, J. Colloid Interface Sci. 483 (2016) 139–145.
[23] Y. Arinicheva, A. Bukaemskiy, S. Neumeier, G. Modolo, D. Bosbach, Studies on thermal and mechanical properties of monazite-type ceramics for the conditioning of minor actinides, Prog. Nucl. Energy 72 (2014) 144–148.
[24] A. Thust, Y. Arinicheva, E. Haussühl, J. Ruiz-Fuertes, L. Bayarjargal, S.C. Vogel, S. Neumeier, B. Winkler, Physical properties of $La_{1-x}Eu_xPO_4$, $0 \leq x \leq 1$, monazite-type ceramics, J. Am. Ceram. Soc. 98 (12) (2015) 4016–4021.
[25] K. Popa, R.J.M. Konings, T. Geisler, High-temperature calorimetry of $(La_{1-x}Ln_x)PO_4$ solid solutions, J. Chem. Thermodyn. 39 (2007) 236–239.
[26] S. Neumeier, Y. Arinicheva, N. Clavier, R. Podor, A. Bukaemskiy, G. Modolo, N. Dacheux, D. Bosbach, The effect of the synthesis route of monazite precursors on the microstructure of sintered pellets, Prog. Nucl. Energ 92 (2016) 298–305.
[27] R. Podor, Raman spectra of the actinide bearing monazites, Eur. J. Mineral. 7 (1995) 1353–1360.
[28] O. Terra, N. Dacheux, F. Audubert, R. Podor, Immobilization of tetravalent actinides in phosphate ceramics, J. Nucl. Mater. 253 (1–3) (2006) 224–232.
[29] R.J.M. Konings, M. Walter, K. Popa, Excess properties of the $(Ln_{2-2x}Ca_xTh_x)(PO_4)_2$ (Ln = La, Ce) solid solutions, J. Chem. Thermodyn. 40 (2008) 1305–1308.
[30] K. Popa, M. Cologna, L. Martel, D. Staicu, A. Cambriani, M. Ernstberger, P.E. Raison, J. Somers, $CaTh(PO_4)_2$ cheralite as a candidate ceramic nuclear waste form: spark Plasma Sintering and physicochemical characterisation, J. Eur. Ceram. Soc. 36 (16) (2016) 4115–4121.
[31] D. Bregiroux, O. Terra, F. Audubert, N. Dacheux, V. Serin, R. Podor, D. Bernache-Assollant, Solid-state synthesis of monazite-type compounds containing tetravalent elements, Inorg. Chem. 46 (2007) 10372–10382.
[32] D. Rai, A.R. Felmy, M.J. Mason, Solubility and ion activity product of $AmPO_4 \cdot xH_2O$, Radiochim. Acta 56 (1992) 7–14.
[33] A.S. Aloy, E.N. Kovarskaya, T.I. Koltsova, S.E. Samoylov, S.I. Rovnyi,

G.M. Medvedev, L.J. Jardine, Immobilization of Am-241, formed under plutonium metal conversion, into monazite-type ceramics, Am. Soc. Mechan. Engin. (2002) 1833–1836.
[34] F. Weigel, H. Haug, Zur Kenntnis des Curium(III)phosphats, Radiochim. Acta 4 (4) (1965) 227–228.
[35] C. Keller, K.H. Walter, Darstellung, Gitterkonstanten und chemische Eigenschaften einiger ternärer Oxide des Plutoniums, Americiums und Curiums vom Typ $Me^{III}X^{V}O_4$, J. Inorg. Nucl. Chem. 27 (1965) 1253–1260.
[36] K.S. Holliday, C. Babelot, C. Walther, S. Neumeier, D. Bosbach, Th Stumpf, Site-selective time resolved laser fluorescence spectroscopy of Eu and Cm doped $LaPO_4$, Radiochim. Acta 100 (2012) 189–195.
[37] D. Bregiroux, R. Belin, P. Valenza, F. Audubert, D. Bernache-Assollant, Plutonium and americium monazite materials: solid state synthesis and X-ray diffraction study, J. Nucl. Mater. 366 (2007) 52–57.
[38] D.E. Hobart, G.M. Begun, R.G. Haire, H.E. Hellwegel, Raman spectra of the trans-plutonium orthophosphates and trimetaphosphates, J. Raman Spectrosc. 14 (1) (1983) 59–62.
[39] C.W. Bjorklund, The preparation of PuP_2O_7 and $PuPO_4$, J. Am. Chem. Soc. 79 (24) (1958) 6347–6350.
[40] R.C.L. Mooney, X-ray diffraction study of cerous phosphate and related crystals, Acta. Cryst. 3 (1950) 337, 240.
[41] A. Mesbah, N. Clavier, E. Elkaim, C. Gausse, I.B. Kacem, S. Szenknect, N. Dacheux, Monoclinic form of the rhabdophane compounds: $REEPO_4{\cdot}0.667H_2O$, Cryst. Growth. Des. 14 (10) (2014) 5090–5098.
[42] A. Mesbah, N. Clavier, E. Elkaim, S. Szenknect, N. Dacheux, In pursuit of the rhabdophane crystal structure: from the hydrated monoclinic $LnPO_4{\cdot}0.667H_2O$ to the hexagonal $LnPO_4$ (Ln = Nd, Sm, Gd, Eu and Dy), J. Solid State Chem. 249 (2017) 221–227.
[43] C.E. Bamberger, R.G. Haire, H.E. Hellwege, G.M. Begun, Synthesis and characterization of crystalline phosphates of plutonium(III) and plutonium(IV), J. Less Common Met. 97 (1984) 349–356.
[44] B. Glorieux, F. Jorion, J.M. Montel, M. Matecki, X. Deschanels, J.P. Coutures, Investigation of plutonium-239 conditioning in monazite and brabantite matrices: synthesis and characterization, O32–04, Proc. ATALANTE 2004, Nîmes Fr. (2004) 1–6.
[45] K. Popa, P.E. Raison, L. Martel, P.M. Martin, D. Prieur, P.L. Solari, D. Bouëxière, R.J.M. Konings, J. Somers, Structural investigations of PuIII phosphate by X-ray diffraction, MAS-NMR and XANES spectroscopy, J. Solid State Chem. 230 (2015) 169–174.
[46] R. Jardin, C.C. Pavel, P.E. Raison, D. Bouëxière, H. Santa-Cruz, R.J.M. Konings, K. Popa, The high-temperature behaviour of $PuPO_4$ monazite and some other related compounds, J. Nucl. Mater 378 (2008) 167–171.
[47] K. Popa, E. Colineau, F. Wastin, R.J.M. Konings, The low-temperature heat capacity of $(Pu_{0.1}La_{0.9})PO_4$, Solid State Commun. 144 (2007) 74–77.
[48] Y. Zhang, E.R. Vance, Plutonium in monazite and brabantite: diffuse reflectance spectroscopy study, J. Nucl. Mater 375 (2008) 311–314.
[49] B.E. Burakov, M.A. Yagovkina, V.M. Garbuzov, A.A. Kitsay, V.A. Zirlin, Self-irradiation of monazite ceramics: contrasting behavior of $PuPO_4$ and (La,Pu)PO_4 doped with Pu-238, Mater. Res. Soc. Symp. Proc. 824 (2004) 219–224.
[50] D. Bregiroux, O. Terra, F. Audubert, N. Dacheux, V. Serin, R. Podor, D. Bernache-Assollant, Solid-state synthesis of monazite-type compounds containing tetravalent elements, Inorg. Chem. 46 (24) (2007) 10372–10382.
[51] X. Deschanels, V. Picot, B. Glorieux, F. Jorion, S. Peuget, D. Roudil, C. Jégou, V. Broudic, J.N. Cachia, T. Advocat, C. Den Auwer, C. Fillet, J.P. Coutures, C. Hennig, A. Scheinost, Plutonium incorporation in phosphate and titanate ceramics for minor actinide containment, J. Nucl. Mater 352 (1–3) (2006) 233–240.
[52] Nirex Report, Review of International Literature on Immobilisation Matrices for Separated Stocks of Plutonium, 2004, p. 106.
[53] S.I. Sinkov, G.J. Lumetta, Sonochemical Digestion of High-fired Plutonium Dioxide Samples, PNNL-16035, 2006.
[54] W.J. Weber, Alpha-irradiation damage in CeO_2, UO_2 and PuO_2, Radiat. Eff. 83 (1–2) (2006) 145–156.
[55] S.S. Hecker, J.C. Martz, Plutonium Aging: from Mystery to Enigma in "Ageing Studies and Lifetime Extension of Materials" by Mallinson, L, Springer, 2001, p. 40.
[56] S.M. Webb, SIXpack: a graphical user interface for XAS analysis using IFEFFIT, Phys. Scr. T115 (2005) 1011.
[57] T. Ressler, WinXAS: a program for x-ray absorption spectroscopy data analysis under MS-windows, J. Synchr. Rad. 5 (2) (1998) 118–122.
[58] A.L. Ankudinov, J.J. Rehr, Relativistic calculations of spin-dependent x-ray-absorption spectra, Phys. Rev. B 56 (1997) 1712–1728.
[59] S. Amelinckx, D. van Dyck, J. van Landuyt, G. van Tendeloo, Handbook of Microscopy, Applications in Materials Science. Solid-state Physics and Chemistry in Applications, VCH Verlagsgesellschaft mbH, Weinheim, 1997.
[60] T. Wiss, H. Thiele, A. Janssen, D. Papaioannou, V.V. Rondinella, R.J.M. Konings, Recent results of microstructural characterization of irradiated light water reactor fuels using scanning and transmission electron microscopy, JOM 64 (12) (2013) 1390–1395.
[61] Y. Hikichi, T. Nomura, Melting temperatures of monazite and xenotime, J. Am. Ceram. Soc. 70 (10) (1987) 252–253.
[62] F. David, Thermodynamic properties of Lanthanide and actinide ions in aqueous solution, J. Less-Common Met. 121 (1986) 27–42.
[63] R.D. Shannon, Revised effective ionic radii and systematic studies of interatomic distances in halides and chalcogenides, Acta Crystallogr. A32 (1976) 751–767.
[64] A. Rossberg, T. Reich, G. Bernhard, Complexation of uranium(VI) with protocatechuic acid – application of iterative transformation factor analysis to EXAFS spectroscopy, Anal. Bioanal. Chem. 376 (5) (2003) 631–638.
[65] D. Prieur, U. Carvajal-Nunez, T. Vitova, J. Somers, Local and electronic structure of americium-bearing PuO_2, Eur. J. Inorg. Chem. 9 (2013) 1518–1524.
[66] H. Funke, A.C. Scheinost, M. Chukalina, Wavelet analysis of extended X-ray absorption fine structure data, Phys. Rev. B71 (2005) 094110.
[67] M. Scavini, M. Coduri, M. Allieta, M. Brune, C. Ferrero, Probing complex disorder in $Ce_{1-x}Gd_xO_{2-x/2}$ using the pair distribution function analysis, Chem. Mat. 24 (2012) 1338–1345.
[68] P. Martin, S. Grandjean, C. Valot, G. Carlot, M. Ripert, P. Blanc, C. Hennig, XAS study of $(U_{1-y}Pu_y)O_2$ solid solutions, J. Alloys Compd. 444 (2007) 410–414.
[69] D.E. Ellis, J. Terra, O. Warschkow, M. Jiang, G.B. Gonzalez, J.S. Okasinski, M.J. Bedzyk, A.M. Rossi, J.G. Eon, A theoretical and experimental study of lead substitution in calcium hydroxyapatite, Phys. Chem. Chem. Phys. 8 (2006) 967–976.
[70] C.M.B. Henderson, S.A.T. Redfern, R.I. Smith, K.S. Knight, J.M. Charnock, Composition and temperature dependence of cation ordering in Ni-Mg olivine solid solutions: a time-of-flight neutron powder diffraction and EXAFS study, Am. Mineral. 86 (2001) 1170–1187.
[71] A.C. Scheinost, D.G. Schulze, U. Schwertmann, Diffuse reflectance spectra of Al substituted goethite: a ligand field approach, Clays Clay Min. 47 (1999) 156–164.
[72] A.C. Scheinost, H. Stanjek, D.G. Schulze, U. Gasser, D.L. Sparks, Structural environment and oxidation state of Mn in goethite-groutite solid-solutions, Am. Mineral. 86 (2001) 139–146.
[73] J.L. Hazemann, A. Manceau, P. Sainctavit, C. Malgrange, Structure of the alpha-$Fe_xAl_{1-x}OOH$ solid solution. 1. Evidence by polarized EXAFS for an epitaxial growth of hematite-like clusters in Fe-diaspore, Phys. Chem. Min. 19 (1992) 25–38.
[74] D. Vantelon, E. Montarges-Pelletier, L.J. Michot, V. Briois, M. Pelletier, F. Thomas, Iron distribution in the octahedral sheet of dioctahedral smectites. An FeK-edge X-ray absorption spectroscopy study, Phys. Chem. Min. 30 (2003) 44–53.
[75] Y. Arinicheva, M.J. Lozano-Rodriguez, S. Neumeier, A.C. Scheinost, N. Clavier, D. Bosbach, Structural studies on (La,Eu)PO_4 solid solutions by infrared, Raman and X-ray absorption spectroscopy, ATAS 2014 (2014).
[76] N. Huittinen, A.C. Scheinost, A. Wilden, Y. Arinicheva, Cm^{3+} incorporation in $La_{1-x}Gd_xPO_4$ monazites: a TRLFS and XAFS study, Ninth Int. Conf. Nucl. Radiochemistry– NRC9 Helsinki, Finl. (2016).